Smart Structures and Systems, *Vol. 27, No. 6 (2021) 903-916*
DOI: https://doi.org/10.12989/sss.2021.27.6.903

Convolutional neural network-based damage detection method for building structures

Byung Kwan Oh [1a], Branko Glisic [2a] and Hyo Seon Park*[3]

[1] *Department of Architectural Engineering, Kyungil University, Gyeongbuk 38428, Republic of Korea*
[2] *Department of Civil and Environmental Engineering, Princeton University, Princeton, NJ 08544, USA*
[3] *Department of Architectural Engineering, Yonsei University, Seoul 03722, Republic of Korea*

(*Received May 17, 2019, Revised April 1, 2021, Accepted April 13, 2021*)

Abstract. This study presents a damage detection method based on modal responses for building structures using convolutional neural networks (CNNs). The modal responses used in the method are obtained from the dynamic responses, which are measured in a building structure under ambient excitations; these are then transformed to a modal participation ratio (MPR) value for a measuring point and mode. As modal responses vary after damages in the structures, the MPR for a specific location and mode also changes. Thus, in this study, MPR variations, which can be obtained by comparing the MPRs of damaged and healthy structures, are utilized for damage detection without the need for identification of modal parameters. Since MPRs are derived for the number of measuring points (N) in the structure as well as the same number of modes (N), the MPRs and MPR variations can be arranged as an $N \times N$ matrix. This low-dimensional MPR variations set is used as the input map of the presented CNN architecture and information about damage locations and severities of the target structure is set as the output of the CNN. The presented CNN is trained for establishing the relationship between MPR variations and damage information and utilized to estimate the damage. The presented damage detection method is applied to numerical examples for two multiple degrees of freedoms and a three-dimensional ASCE benchmark numerical model. Training datasets created from damage scenarios assuming changes in the stiffness are used to train the CNN and the performance of this CNN is verified. Finally, this study examines how variations in the operator size and number of layers in the CNN architecture affect the damage detection performance of CNNs.

Keywords: structural health monitoring; damage detection; convolutional neural network; dynamic response; modal participation ratio

1. Introduction

In the past, various studies have been conducted using advanced sensing technologies to evaluate and analyze the health of structures; these studies and techniques fall under the aegis of structural health monitoring (SHM) (Sigurdardottir and Glisic 2014, Kaveh and Maniat 2015, Oh *et al*. 2015, Park *et al*. 2017, Sotoudehnia *et al*. 2019). In particular, SHM includes methods for measuring structural responses using sensors installed on structures and diagnosing structural health using these measured responses. Vibration-based SHM is one such technique that is used to measure vibrational responses from structures; these responses can convey unique characteristics regarding these structures, which, in turn, can be used to identify their structural conditions and evaluate safety. Modal parameters, which are inherent characteristics of structures, can be obtained through the vibration-based SHM technique using various types of dynamic structural responses (Glisic and Inaudi 2012, Park *et al*. 2015, Xiong *et al*. 2019) in order to evaluate the health of these structures. These techniques for extracting, analyzing, and evaluating modal parameters have also been applied to high-rise as well as other large structures (Glisic *et al*. 2013, Li *et al*. 2017, Zhu *et al*. 2018). Furthermore, the extracted modal parameters can be utilized to identify locations and evaluate severities of structural damages in various ways (Hsu *et al*. 2017, Liang *et al*. 2017, 2019).

In particular, studies on damage detection using modal parameters, such as natural frequency, mode shape, and modal damping, that are extracted from vibration measurements, are largely classified into those based on model updating (MU) and those based on artificial neural networks (ANNs). Among these, the studies on MU-based damage detection primarily involve setting the difference between the modal parameters extracted from the damaged structures through structural measurements and modal parameters of a finite element (FE) model for the target structure as the error or objective function; in addition, they also include the determination of structural parameters related to stiffness and mass that minimize this error function. Then, they find the damage location and severity by investigating the variations of rotational stiffness (Yin *et al*. 2017), story stiffness (Chen and Loh 2018), and flexural rigidity (Esfandiari 2017) in the FE model reflecting the searched structural parameters.

*Corresponding author, Ph.D., Professor,
E-mail: hspark@yonsei.ac.kr

ISSN: 1738-1584 (Print), 1738-1991 (Online)

ANN-based damage detection methods involve specifying the relationships between the modal parameters that can be changed owing to damage and damage information including damage location and severity in advance under damage scenarios for the target structure through ANN training. Thus, when actual damage occurs in the future, only modal parameters obtained from measurements are used to estimate the damage. Many types of ANN models have been developed to estimate damages by investigating the relationship between the change in modal parameters and changes in other parameters, such as elastic modulus (Padil *et al*. 2017), mass and stiffness (Zhang and Xu 2016), and flexural stiffness (Li *et al*. 2015) of a structure.

Although modal parameters have been used for SHM in various ways because they reflect the inherent characteristics of structures, many uncertainties are involved in the process of extracting the values (Park and Oh 2018a). For example, when a real-world structure is considered, the vibration responses need to be measured to extract modal parameters, which requires a field test; accordingly, modal parameters are affected by the external conditions of the field tests. Some previous studies have showed that natural frequency and modal damping values changed according to the amplitude level of the vibration measurements (Guo *et al*. 2016, Sarlo *et al*. 2018). Moreover, in an ambient vibration test, the values of the modal parameters changed because of temperature and humidity as well (Zhang *et al*. 2016, Wu *et al*. 2018). These uncertainties experienced during the extraction of modal parameter values cause difficulties in developing a damage detection model based on modal parameters.

Thus, to overcome the difficulty of accurately extracting modal parameters, damage detection methods that do not use modal parameters have been developed. In particular, in some studies, researchers have proposed damage detection methods that directly use time series structural responses measured in structures (Xu *et al*. 2011, Machavaram and Shankar 2013, Li and Hao 2014). These methods do not require the extraction of modal parameter values, thereby avoiding the related uncertainty. However, these methods require loading information to extract the time history of structural responses. Therefore, though these methods are applicable to small-scale structures, and have limitations for application in complex and large civil infrastructure or buildings because, in such cases, the application of loading is either difficult, impossible, or costly.

Considering this, in another group of studies, researchers developed damage detection methods for structures under ambient excitation conditions (Abdeljaber *et al*. 2017, 2018, Lin *et al*. 2017, Sun *et al*. 2017); these studies use time series structural responses measured in ambient vibration tests for damage detection. To obtain the inherent characteristics from the vibration responses of a structure under ambient excitation, sufficient measuring time and quantity of structural response data are required; this is especially true in the case of a complex/large structures, for which, an enormous quantity of measurement data is necessary. Therefore, damage detection methods using time series structural responses have used machine learning techniques to suitably handle such voluminous measurement data. Among the many machine learning techniques available, the convolutional neural network (CNN) technique, which is a deep learning strategy, is widely used in studies related to SHM (Park *et al*. 2018). As CNN was modeled after the visual cortex of animal, it was initially applied to the field of image recognition (Lecun *et al*. 2015). In addition, in the civil engineering domain, many studies introduced CNN for image-based crack detection (Xu *et al*. 2018, Chen and Jahanshahi 2018).

Because CNNs do not need require handcrafted data extraction, this solves the overfitting problem efficiently (Chen *et al*. 2018), thus making CNNs suitable for handling noisy data as well. In addition to crack detection, CNNs are actively applied to damage detection for structures using time series structural responses. Abdeljaber *et al*. (2017) applied a one-dimensional (1-D) CNN to estimate the damage locations of a steel structure under unknown input excitation conditions; in their proposed CNN, time history acceleration responses of the structure before and after damage were set as input, while the damage probability of the steel frame joint was the output. Their proposed method was verified by conducting a random excitation experiment for a steel structure. Furthermore, Lin *et al*. (2017) applied a 1D-CNN for damage detection of a beam-like structure under random excitation. In particular, they proposed a CNN model that uses the low-level waveform time series of acceleration measured in a structure before and after damage as input, producing the damage locations as output. In addition, they attempted to obtain physical insight into the learning process within their CNN by visualizing its hidden layers. Their proposed method was verified through a numerical study. Sun *et al*. (2017) proposed a CNN-based virtual sensing structural model. In this study, a two-dimensional (2-D) CNN with time history acceleration responses measured for a structure under white noise excitation as input, and time history acceleration responses of specific positions in the structure as output, was presented. Their proposed method was verified by conducting an experimental study for a simple beam as well as a numerical study for multiple degrees of freedom (MDOFs) and a cantilever beam; their method showed good performance for damage prediction. Because the CNN training was performed for specified loading conditions in their study, it is believed that this method would not work under different conditions. Furthermore, Abdeljaber *et al*. (2018) introduced a 1-D CNN to detect damages in a steel structure using time history acceleration responses as input, and generating the overall damage severity of the structure as output. The overall damage information is evaluated based on the number of structural components that were completely damaged; this method requires only the measurement of healthy and fully damaged states but cannot identify damage locations.

These abovementioned studies developed efficient damage detection methods for structures under ambient or random excitation without extracting modal parameters. Since they were limited to either damage localization (Abdeljaber *et al*. 2017) or damage severity (Abdeljaber *et al*. 2018), they have difficulties in comprehensive damage

detection. In addition, the prediction performance of these methods is not suitable in the case of multiple damage detection (Abdeljaber *et al*. 2017, Lin *et al*. 2017). For example, Abdeljaber *et al*. (2017) accurately predicted single damage locations through their 1D-CNN, but showed faulty detections in two cases involving five double damage localizations wherein undamaged joints were estimated as damaged. Furthermore, the model proposed by Lin *et al*. (2017) failed to predict damage or showed faulty detection in some multiple damage detection cases. Thus, although the CNNs might have been built by efficiently acquiring structural features from large-scale time history structural responses, it is not certain that essential features, including the unique characteristics of structures, are consistently and accurately reflected because the structural responses under random excitation were directly used for constructing the CNN. In particular, when two cases, one including and another not including noisy data in training, were compared in a study on CNN-based damage detection (Lin *et al*. 2017), for the case with noisy data, the accuracy was 86.99% even with single damage detection; this indicates that the noise problem is not fully solved by these previously proposed CNN-based damage detection methods. In addition, it still needs to be verified whether the CNN constructed in a random excitation condition will work under other ambient excitation conditions. In particular, though it is reasonable to use random excitation conditions to build a CNN in the case of the above studies, the measurements obtained at a different time (such as at an estimated time of damage) in a structure under ambient excitation conditions cannot be the same as the structural responses used for CNN training in the abovementioned studies. This is because ambient responses are affected by various internal (number, activity type, and amount of activity of occupants in the structure and type and quantity of operation of internal machines in the structure) and external factors (direction and speed of wind and traffic conditions around the structure) of a structure, i.e., they are created randomly. Thus, in order to use time history structural responses for damage detection, further studies are required that account for practical issues that can affect real-world structures.

This study presents a CNN-based damage detection method for building structures under ambient excitations using the modal participation ratio (MPR), which is extracted from time history modal responses. Because the MPR includes mode information of a target structure at a specific location, it can be used for identifying the unique features of a structure such as damage locations and severities. Thus, the presented method does not require conventional extraction process of modal parameters such as mode shape and modal damping ratio which can be largely influenced by many uncertainties in the field tests. In addition, as modal responses to obtain the MPR are extracted by using a robust and fast filtering in this method, noises in the dynamic responses by many internal and external factors in the ambient excitation tests can be removed and more clear modal characteristics are reflected from dynamic responses to both modal responses and MPR. Under the assumption that the number of measuring points (N) is equal to that of the modes considered (N), this study obtains as many modal responses as the considered modes from the measurements of structural responses at each measuring point of the structure, thus extracting MPRs from modal responses. Therefore, the total number of MPRs used is $N \times N$. MPR variations are defined as the relative difference between the MPRs of a damaged structure and those of a healthy structure; those low-dimensional MPR variations are used as the input of the presented CNN. In the CNN, the damage information of the structure, such as location and severity of damage, which can be expressed as stiffness reduction at the damage location, is set as output. In addition, CNN training is conducted using input/output information of large training datasets that have been created according to a predefined scenario. Although the MPR extraction from structures under ambient excitation conditions is simple, pre-processing for measured time history data is required to prevent the effect of noise on the measured data during CNN training; in general, this pre-processing is not time-consuming, but requires robust and fast filtering. Through the pre-processing using band-pass filtering with modes under consideration, more clear modal behaviors can be reflected in the damage detection by removing some noises from the field tests. In addition, time history responses are not directly used; however, to better reflect behaviors of a building under various load-related circumstances into responses used in the damage detection, a sufficient length of ambient excited dynamic responses is considered in the MPR extraction based on the fact that MPR value converges according to the increase of length of data used in the MPR extraction (Park and Oh 2018b). Thus, in this method, the MPR values stably obtained from a sufficient quantity of ambient response data are used for the CNN training to overcome the limitations of the conventional CNN-based damage detection methods that directly used limited length of time series responses data. Since time series data are not directly used, and instead MPR values, whose number is as small as those of the considered modes and DOFs (the number of acceleration-measuring axes), are used as input, the CNN training was considerably more efficient than the previous cases; in particular, the results of multiple damage detection were highly accurate. Furthermore, the presented method is applied to a numerical study on damage detection with 12- and 20-MDOFs. To train the CNN, 1000 training sets are created by varying the story stiffness of the MDOFs; another 100 data sets, which have not been used for the CNN training, are used to verify the performance of the presented method for detecting single and multiple damages. In addition, the presented method is also applied to a numerical study on damage detection of a 3-D four-story steel structure, i.e., the ASCE benchmark model. In the case of multiple damages, for CNN training, 3000 multiple damage scenarios are generated by varying the stiffness of the brace; another 100 data sets, which have not been used for training, are applied to analyze the applicability of the presented method for multiple damages. Moreover, the damage detection performance of the presented CNN is examined according to changes in parameters of convolutional and pooling layers of the CNN,

such as size of the operator and number of layers, which are then evaluated in terms of estimation accuracy and computational costs.

2. Methodology

The CNN-based damage detection method for building structures presented in this study uses big datasets created under predefined damage scenarios for CNN training. As previously mentioned, in the CNN, an MPR extracted from measured structural modal responses is set as the input layer, whereas damage locations and damage severity are set as the output layer. In particular, damage is predicted using structural modal responses measured at times of its occurrence.

2.1 MPR extraction

Instead of directly using time series responses measured from the structure in the CNN input layer, this study extracts an MPR from the modal responses of a structure under ambient excitation conditions, which is then used in the input layer of the CNN. As is known from existing literature on vibration-based MU (Oh *et al*. 2017) methods, the degrees to which each mode participates in the structural response are different; these degrees can be defined as the modal participation mass ratio. In a similar manner, modal responses obtained from measured structural responses also show different degrees to which each mode participates in structural behaviors. Because the MPR is extracted from modal responses measured at a specific location in a structure, it reflects the features of each mode at the particular measuring point. If a target structure has different behavioral characteristics depending on the damage characteristics, the modal response obtained at each mode and measuring point also varies (Oh *et al*. 2017). Thus, considering that the MPR value for a specific location and mode changes according to different damage characteristics, this study aims at constructing a CNN for damage detection of a structure using MPR values that are sensitive to both the damage location and severity. To include modal behavioral characteristics into damage detection, MPR values which change with different trends depending on locations in the structure and modes are required as many as the numbers determined by the number of locations to be monitored and modes under consideration. Since those relatively large number of MPR values are used in the input information of the presented method, the CNN which is able to constitute the large size of input map is more suitable for employing those MPRs rather than the conventional artificial neural network. Fig. 1 illustrates the MPR extraction process.

As shown in Fig. 1(a), the time history dynamic structural responses, which are considered accelerations in this study, are measured for the target structure under ambient excitation. The measuring time and sampling rate are sufficiently and suitably set to better reflect dynamic behaviors of the structure and stably extract the MPR vale during the measurement of time history acceleration responses. The dynamic structural responses, which are equal in number to the considered measuring points, are divided into modal responses as the same number of considered modes using band-pass filtering (Oppenheim and Schafer 2011) for each measuring point; this process is described via Eqs. (1)-(3). This filtering acts on extraction of modal responses including more clear modal characteristics by removing noise in the measured dynamic responses. For example, assuming that structural responses are measured at each story of a 12-story structure, the process of obtaining the modal responses from structural responses measured on the highest floor is shown in Fig. 1(b).

$$A^j(f) = \int_{-\infty}^{\infty} a^j(t)\, exp(-i\omega t)dt \quad j = 1 \;\; to \;\; n_s \tag{1}$$

$$A_i^j(f) = H_i^j(f)\{A^j(f)\} \quad i = 1 \;\; to \;\; n_m j = 1 \;\; to \;\; n_s \tag{2}$$

$$y_i^j(t) = \frac{1}{2\pi}\int_{-\infty}^{\infty} A_i^j(f)\, exp(ift)df \quad i = 1 \;\; to \;\; n_m j = 1 \;\; to \;\; n_s \tag{3}$$

where $a^j(t)$ is the time history of the acceleration response of the j-th DOF, $A^j(f)$ is the response of the j-th DOF in the frequency domain, n_s is the number of stories

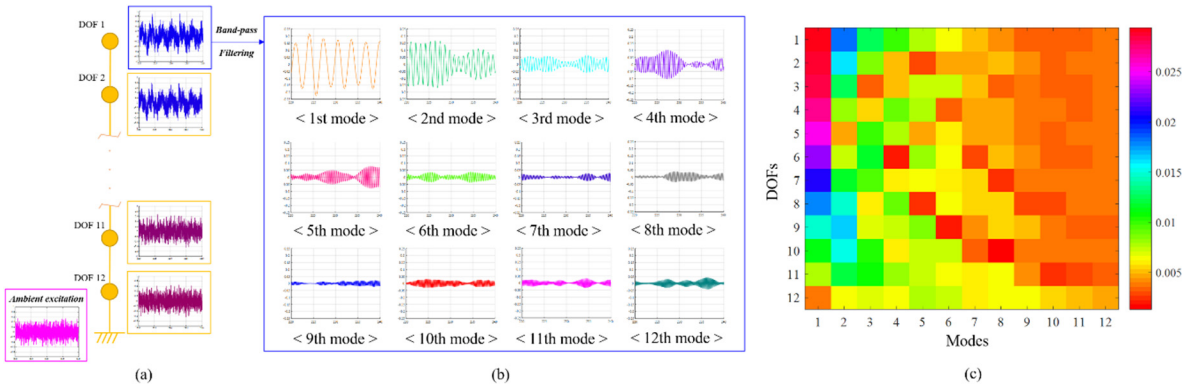

Fig. 1 Procedure for MPR extraction: (a) time history responses of 12-DOFs under ambient excitation conditions; (b) the first 12 modal responses for DOF 1; (c) MPR map for all modes and all DOFs

or DOFs to be considered, i.e., the number of measurement locations, and $H_i^j(f)$ is the transfer function of the band-pass filter for the i-th mode of the j-th DOF.

The natural frequencies for the considered modes required in the selection of filtering range can be identified by frequency domain analyses for the time histories of the acceleration responses considering locations and axes of sensors installed in the structure. $A_i^j(f)$ is the filtered response of the i-th mode of the j-th DOF in the frequency domain, n_m is the number of modes considered, and $y_i^j(t)$ is the modal response of the i-th mode of the j-th DOF in the time domain.

From the obtained modal responses, the root mean square of the modal response (RMSMR) for each DOF and mode is obtained, as described by Eq. (4). This study defines MPR as the ratio of an RMSMR for a particular DOF and mode to the total RMSMR for all DOFs and modes; this is represented by Eq. (5). As specified in the abovementioned example, if the MPR is calculated for 12 DOFs, a total of 144 MPRs can be obtained for 12 DOFs and 12 modes from modal responses using Eqs. (4)-(5); these are shown in Fig. 1(b). The MPR map obtained from those 144 MPRs is shown in Fig. 1(c).

$$RMSMR_i^j = \sqrt{\frac{\sum_{k=1}^{l} y_i^j(k)^2}{l}} \quad i = 1 \;\; to \;\; n_m j = 1 \;\; to \;\; n_s \tag{4}$$

$$MPR_i^j = \frac{RMSMR_i^j}{\sum_{i=1}^{n_m}\sum_{j=1}^{n_s} RMSMR_i^j} \quad i = 1 \;\; to \;\; n_m j = 1 \;\; to \;\; n_s \tag{5}$$

where $RMSMR_i^j$ is the RMSMR for the i-th mode of the j-th DOF, l is the length of the measured data, and MPR_i^j is the MPR for the i-th mode of the j-th DOF. Based on this definition, indicates the contribution of the i-th mode of the j-th DOF on the structural responses in a quantitative manner. Therefore, the MPR thus obtained can reflect the behavioral characteristics of the target structure, which has different response distributions for each mode and location depending on the locations and severities of damage. Considering these MPR characteristics, this study used MPR as the input of CNN for damage detection.

2.2 CNN architecture

Using the MPR extraction process discussed in the previous section, the MPRs are extracted from both healthy and damaged structures; in particular, the variation between these two MPRs is used as the input for the presented CNN.

The MPR variation is calculated at each mode and for each DOF using the following equation

$$\Delta MPR_i^j = \frac{DMPR_i^j - HMPR_i^j}{HMPR_i^j} \times 100 \quad i = 1 \;\; to \;\; n_m j = 1 \;\; to \;\; n_s \tag{6}$$

where ΔMPR_i^j, $HMPR_i^j$, and $DMPR_i^j$ are the MPR variation, MPR of the healthy structure, and MPR of the damaged structure of the i-th mode of the j-th DOF, respectively. The MPR variation was examined using the example of 12 DOF previously presented in the previous section. The MPR variations for 30% stiffness reduction in the case of DOF 1, which represents the top story of the 12 DOF structure, and in DOF 12, i.e., the lowest story, are

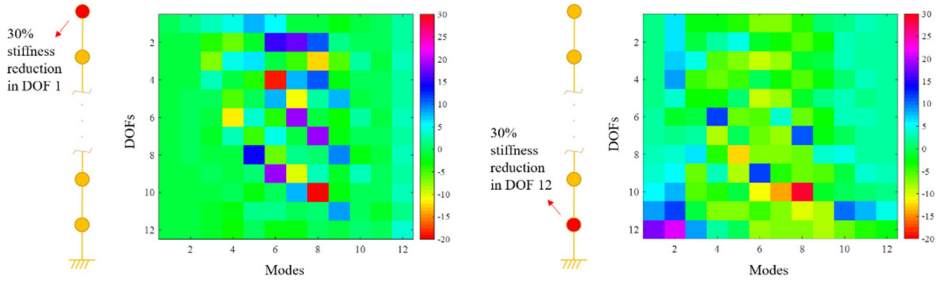

Fig. 2 MPR variations in case of (a) 30% stiffness reduction in DOF 1; (b) 30% stiffness reduction in DOF 12

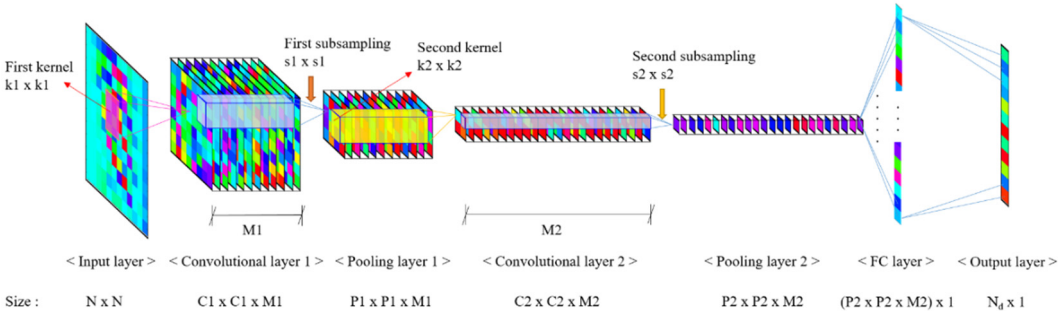

Fig. 3 Presented CNN architecture

illustrated in Figs. 2(a) and (b), respectively. As the figure shows, the MPR variations for each mode and DOF have different values depending on the damage location.

Fig. 3 shows the presented CNN architecture with the MPR variation obtained using modal responses as input. In the input layer, the MPR variations are set to the same number as there are considered modes or measuring points, i.e., the number of DOFs. The primary characteristic of the input layer of the presented architecture is that the number of considered modes (n_m) is equal to that of the considered measuring points (n_s), i.e., *N*. Therefore, the map of the input layer as well as hidden layers is square-shaped.

As shown in Fig. 3, the hidden layers of the presented CNN architecture are set by consecutively arranging convolutional and pooling layers twice. The second pooling layer is connected to the FC layer. Finally, the FC layer is connected to the output layer. In Fig. 3, *N* is the number of considered modes for MPR extraction; as previously mentioned, this value is equal to the number of measuring points. *C*1 and *C*2 are the sizes of the first and second convolutional layers, respectively, while *P*1 and *P*2 indicate the sizes of the first and second pooling layers, respectively. Furthermore, *M*1 and *M*2 indicate depths of the first and second convolutional (or pooling) layers, respectively. N_d is the number of damage locations considered. In addition, *k*1 and *k*2 are the sizes of the kernels used to construct the first and second convolutional layers, respectively. *s*1 and *s*2 are the subsampling sizes used to construct the first and second pooling layers, respectively. In general, the presented CNN architecture is similar to a typical CNN; therefore, the functions and characteristics of each layer are the similar to those reported in existing literature on CNNs (Abdeljaber *et al*. 2017, 2018, Lin *et al*. 2017, Sun *et al*. 2017) while the presented method mainly focusses on constitution of input map in CNN based on the relationship between MPR and damage. Since extracted MPRs (as many of them as the number of locations and modes under consideration from dynamic responses with sufficient lengths) are set as input map in the CNN, the size of input map in the presented CNN can be significantly reduced compared with the other methods identified in aforementioned literature on CNN-based damage detection, which established time history data of structural responses as input map in the CNN. The presented CNN with low-dimensional input map results in significant reduction of computational costs. In the case of missing MPRs due to failure in identification of some modes, zero padding can be used to fill the locations of MPR variations for unidentified modes in the input map. While the performance of CNN in detecting damage will be altered by missing MPRs and their replacement with zero padding, the alteration does not reduce the performance of CNN significantly.

During the CNN training, through filtering by the first kernel, the MPR variation, which forms the input map, generates a convolutional layer with the depth of first layer. In this case, the size of the convolutional layer (*C*) is calculated using the following equation

$$C = \frac{(I - k)}{C_{st}} + 1 \tag{7}$$

Table 1 Details of the presented CNN architecture

Type	Size
First kernel (k1 × k1)	5 × 5
First subsampling (s1 × s1)	2 × 2
First output map size (M1)	12
Second kernel (k2 × k2)	3 × 3
Second subsampling (s2 × s2)	2 × 2
Second output map size (M2)	24

where *k* is the kernel size for filtering the input map and *Cst* is the stride size, i.e., the interval of convolution of the kernel. To obtain the size of the first convolutional layer (*C*1), the input size *N* is substituted for *I* in Eq. (7). Similarly, to obtain the size of the second convolutional layer (*C*2), the size of the first pooling layer is substituted for *I* in Eq. (7). After the convolutional layers are generated, the pooling layers are created by subsampling. The size of a pooling layer (*P*) is calculated using the following equation

$$P = \frac{(I - s)}{P_{st}} + 1 \tag{8}$$

where *s* is the subsampling size and *Pst* is the stride size in the pooling layer. The size of the first pooling layer (*P*1) as well as second pooling layer (*P*2) are calculated in the same manner as the convolutional layers, but with alternative layers, using Eq. (7). As previously mentioned, the last pooling layer is connected to a FC layer; the size of the FC layer is determined by multiplying the square of the size of last pooling layer by the depth of the last pooling layer. Finally, the FC layer is connected to the output layer. The size of the output layer (N_d) indicates the number of damage locations considered in the damage scenarios that are used for creating the training datasets for a damaged structure. Each node of the output layer indicates a damage location and the value of each node is set to a value that indicates the severity of the damage.

Table 1 lists the depth and values of operators used in each layer of the presented CNN. The presented CNN architecture, which has these specified values as default values, is applied for damage detection to two MDOFs, which is discussed in Section 3, and a three-dimensional (3-D) steel structure, which is discussed in the Section 4. The pooling type in the pooling layer is average pooling. A sigmoid function was used as the activation function in the convolutional and FC layers. The learning rate was set to 1.0 and the training termination condition was set to 1000 epochs. The CNN of the presented method was implemented in Matlab.

3. Numerical example

The presented CNN-based damage detection method is applied to a numerical study for damage detection with two MDOFs. The previously mentioned examples included 12- and 20-DOFs, which represents the same shear type

structure as the model in Fig. 1(a). These two examples are assumed to be 12- and 20-story structures, respectively. It is also assumed that sensors are installed on each floor to obtain measurements for the 12 and 20 DOFs, respectively. In addition, because of the number of assumed DOFs, 12 and 20 translational modes are considered for damage detection in the two examples, respectively. In both examples, a mass between 1.0 kg and 1.5 kg is distributed on each story and the stiffness of each floor is assumed to be 300 N/m. Furthermore, a 2% modal damping is considered for each considered mode in these examples.

3.1 Damage scenario

To apply the presented damage detection method to the example structures, CNN training datasets were created. In particular, the damage was expressed as the story stiffness reduction of each story. The stories undergoing stiffness reduction were randomly selected in creating the training datasets. The stiffness reduction ratio of each story was also randomly assigned. In this manner, a total of 1100 damage scenarios were prepared. The story stiffness reduction ratio was set to be between 0% and 30%. The damage is considered as small based on real-life examples from literature (Sigurdardottir and Glisic 2015). Given that damage was small, non-linear effects that it introduces were neglected. Based on the damage scenarios, the dynamic analysis subject to white Gaussian noise excitation was conducted for each example to construct the CNN training datasets. In the dynamic analyses, Newmark-beta method was used (Chopra 2001). Even if white Gaussian noise was included to simulate ambient excitation, various uncertainties such as colored excitation which is often found in the actual ambient excitation were not comprised in the excitation. Since the band-pass filtering, which is included in the presented method, enables to obtain clear modal responses from the noisy responses measured in the ambient vibration field test (as per previous work (Park and Oh 2018a)), employing the white Gaussian noise excitation was judged as suitable for the validation of the presented method based on the filtering. The acceleration responses of each story of each example structure obtained using this dynamic analysis subject to white Gaussian excitation were used to extract the MPRs. The MPR of the damaged structure was compared with that of a healthy structure to obtain the MPR variation. The obtained MPR variation was set as the input of the CNN, whereas the damage location and damage severity of each damage scenario were set as the output. These input and output were included in a single dataset, which was then used for CNN training.

3.2 Single damage detection

The applicability of the presented method was verified for single damage detection of the abovementioned two example structures. When damage scenarios were generated, the number of stiffness reduction stories, which is randomly selected, was set to 1, and the stiffness of the damaged story is reduced by a randomly chosen value between 0% and 30%. In this way, total 1100 CNN training datasets were created. Among the 1100 datasets, 1000 datasets were used for CNN training, while the remaining 100 datasets were used to verify the trained CNN. Figs. 4(a) and 4(b) show the verification results for the cases of 12 DOF and 20 DOF, respectively.

Among the 100 datasets, the results for the five most unfavorable datasets in terms of absolute error in predicting damage are shown in the figure. The 100 verification datasets for 12 DOF and 20 DOF cases had RMSEs of 0.2761 and 0.2642, respectively, and average absolute errors of 0.1260 and 0.1137, respectively. In general, the presented CNN model showed accurate estimations of damage location and damage severity for the datasets of the damage scenarios, which had not been used for training. Although the results shown in Fig. 4 are for the most unfavorable cases, they show no faulty damage detection. However, in the third case shown in Fig. 4(b) with a 3%

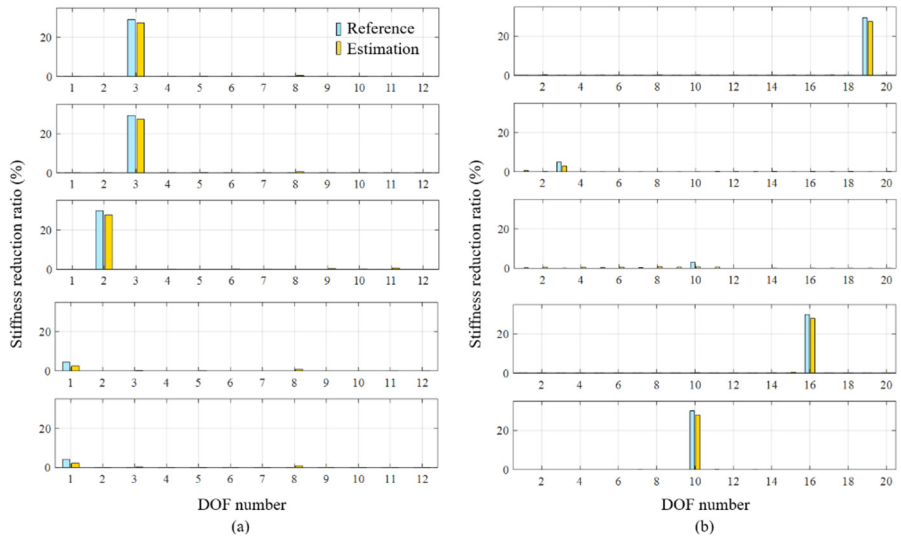

Fig. 4 Single damage detection results for the five most unfavorable verification datasets for (a) 12 DOF structure; (b) 20 DOF structure

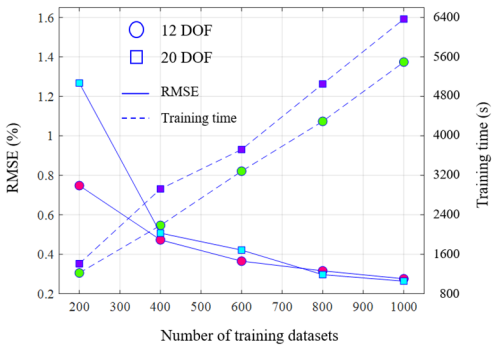

Fig. 5 Relationship between the number of training datasets with RMSE and training time

story stiffness reduction in DOF 10, accurate estimation of damage is not obtained. In general, cases with lower rates of story stiffness reduction were more likely to have erroneous estimation of damage. However, this loss of stiffness is practically very low and in general damage of this size does not represent important alteration of structural health and performance in real structures (Sigurdardottir and Glisic 2015).

As shown in Fig. 5, although increasing the number ofdatasets used for the training decreased the error of CNN estimation, the differences of RMSEs for 12 and 20 DOFs between the cases with 400 and 1000 training datasets were not significant, which were 0.1969 and 0.2431, respectively. Nevertheless, increase of the number of training datasets can be expected to slightly improve the damage detection performance of CNN. Meanwhile, when more datasets were used for the CNN training, the computational cost inevitably increased.

3.3 Multiple damage detection

The applicability of the presented method was verified for double damage detection for the two example structures. To create damage scenarios for double damage detection, two stories were randomly selected for stiffness reduction, and the stiffness reduction ratios of the selected two stories are randomly set to the values between 0% and 30%. Eventually, 1100 datasets for double damage were created for CNN training. Among the 1100 datasets, 1000 datasets were used for CNN training, while the remaining 100 datasets were used to verify the trained CNN. In general, the presented CNN model showed accurate estimations of damage location and damage severity for the datasets of the damage scenarios, which had not been used for training. Furthermore, the 100 verification datasets for the 12 DOF and 20 DOF cases had RMSEs of 0.9503 and 1.1658, respectively, and average absolute errors of 0.5365 and 0.4783, respectively. It was observed that the performance of double damage detection was significantly lower than that of the single damage detection both in terms of RMSE and absolute error. Figs. 6(a) and 6(b) show the results for the five most unfavorable datasets in terms of absolute error in predicting damage among the 100 verification results for the 12 DOF and 20 DOF cases, respectively.

Among the 100 verification sets of 12 DOF, the five most unfavorable cases with highest error values showed absolute errors ranging from 6.16 to 7.98. Although these cases tended to underestimate damage severity (red circle in Fig. 6(a)), there was no faulty detection. In contrast, among the 100 verification sets for the 20 DOF case, the set with the highest error showed faulty detection (blue dotted circle in Fig. 6(b)) with an absolute error of 18.08. Some faulty detections were observed in DOF 2 and 15 (green circle in Fig. 6(b)); those were false positive. Aside from this observation, in the remaining four cases, multiple damage locations were accurately predicted, but the model tended to underestimate the damage severity. Thus, even though Fig. 6 with the five most unfavorable cases showed inaccurate results, the damages were relatively precisely estimated in the remaining 95 cases without faulty detection. Considering this, the presented CNN seems to be suitable for double damage detection based on the analysis of all verification sets. Though not discussed in this section, a further study showed that the increase in the number of

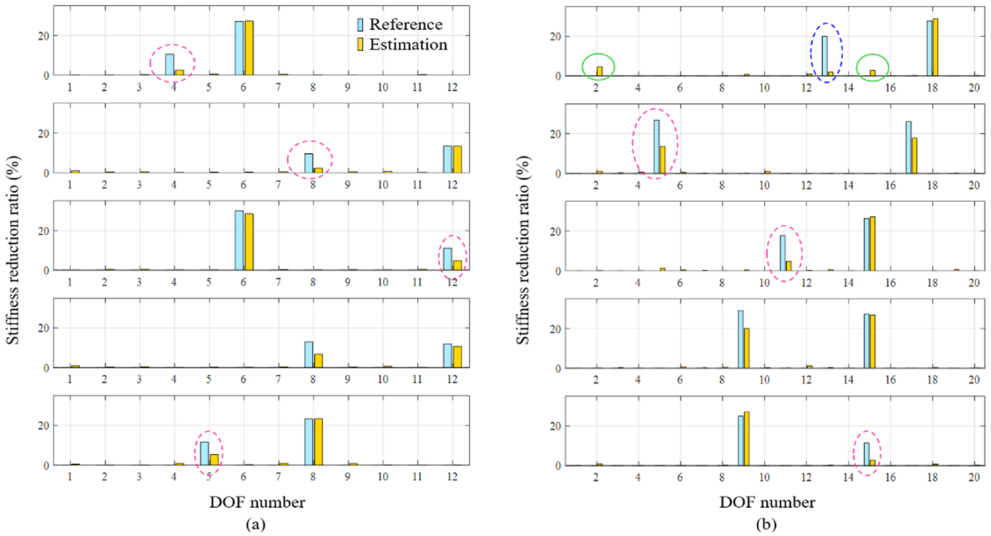

Fig. 6 Multi-damage detection results for the five most unfavorable verification datasets for (a) 12 DOF structure; (b) 20 DOF structure

training datasets could improve the performance of CNNs for double damage detection.

4. Evaluation using the ACSE benchmark model

The presented CNN-based damage detection method was used to identify the damages of a 3-D ASCE benchmark numerical model (Fig. 7). The target structure was a 4-story and 2 bay-by-2 bay steel structure with a floor plan of 2.5 m × 2.5 m and a total height of 3.6 m. This experimental specimen is a benchmark model for SHM research, which was first proposed by ASCE (Johnson *et al*. 2004). It has been widely used to verify methods proposed by many SHM-related studies on MU, system identification, and damage detection (Abdeljaber *et al*. 2018). The target structure was composed of columns, beams, slabs, and braces, all of which were made of hot rolled 300 W steel with a material property of 300 MPa nominal yield stress. The beams, columns, and braces had sections of S75 × 11, B100 × 9, and L25 × 25 × 3, respectively. The section properties and other detailed information about the structure are presented in the following reference (Johnson *et al*. 2004).

Fig. 7 ASCE benchmark model

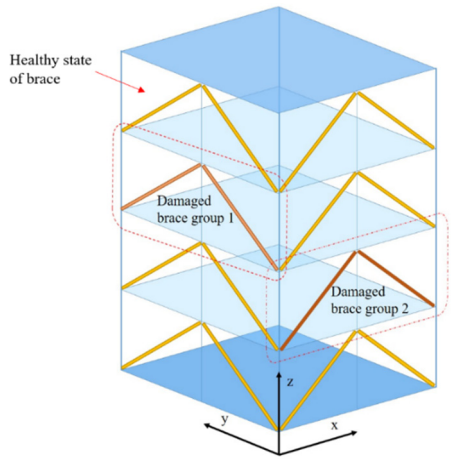

Fig. 8 Description of damaged brace groups for damage detection in the ASCE benchmark model

4.1 Damage scenario

To apply the presented CNN-based damage detection method to the ASCE benchmark specimen, damage was assumed to occur in a total of 32 braces installed in the structure. These braces were the target structural components for damage detection. The damaged structure with lower lateral stiffness was constructed by modifying the axial stiffness of the brace. Since the variations in mass by the changes of cross-sectional area of the brace for reducing the axial stiffness were negligible compared with the value of mass in each slab (Johnson *et al*. 2004), mass changes by the brace were not included in the model. As shown in Fig. 8, two braces installed in one direction on one story were considered as one group; for simplification purposes, the two braces of the same group were assumed to have the same stiffness. Therefore, a total of 16 brace groups were set as the targets for damage detection. The damage scenario assumed multiple damages, i.e., stiffness reduction in two brace groups. Two randomly selected groups were considered for stiffness reduction according to a random reduction ratio (orange and red brace groups in Fig. 8). The stiffness reduction ratios of the selected two brace groups were randomly set between 0% and 30%. The remaining 14 brace groups retained their initially assigned stiffness (yellow brace group in Fig. 8).

Thus, a total of 3100 damage scenarios were created, of which 3000 scenarios were used for CNN training, while the remaining 100 scenarios were used to verify the damage detection performance of the CNN. Even if the damage severities of training and verification damage scenarios were randomly assigned, the ratios of the damage cases which exceeded 25% of damage severities were similar for both training and verification scenarios. By employing those imbalanced datasets in the verification, the practical implementations including the extreme damage conditions were considered. To generate the training and verification datasets, the damaged structures were modeled according to the given damage scenarios; then, time history acceleration responses were extracted using dynamic analysis. Under the assumption that the measurement was conducted under ambient excitation conditions, time history acceleration responses of the damaged structure were obtained by applying bi-axial white noise for 600 s. OpenSees (PEER 2006) was used for the structural modeling and dynamic analysis. In OpenSees modeling, material properties presented in the literature (Johnson *et al*. 2004) were assigned to all elements. Columns and beams were modeled using elastic beam-column element and braces were modeled by using truss elements. Rigid diaphragm was assigned to each story and additional mass which detail is presented in the literature (Johnson *et al*. 2004) was applied to each story. When extracting the MPR from the obtained time history acceleration responses, 12 modes were considered, including four degrees of x-translation modes, y-translational modes, and torsional modes, each. Furthermore, a total of 12 DOFs were considered, of which 3 DOFs were considered for the x, y, and torsional directions on each floor, corresponding to the 12 DOFs for

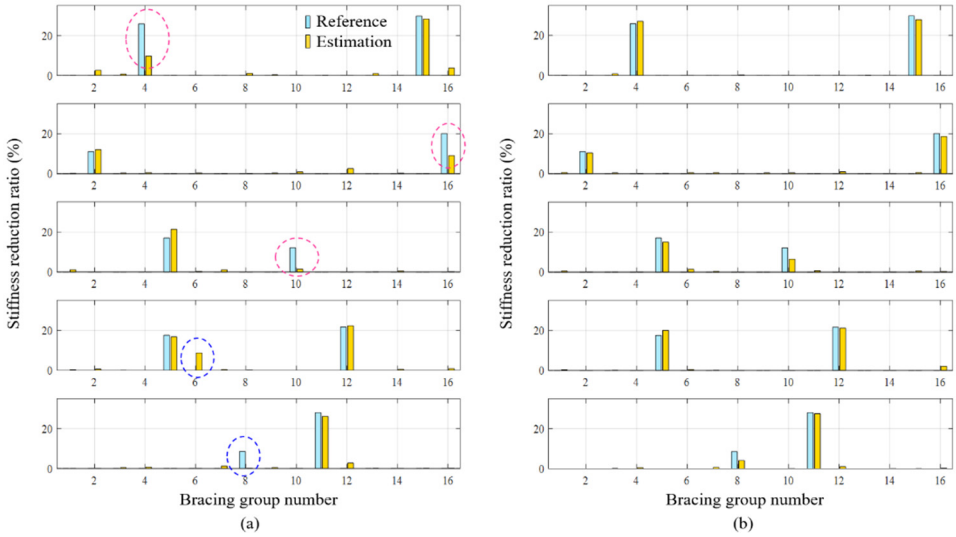

Fig. 9 Five most unfavorable verification datasets for damage detection in the ASCE benchmark model using (a) 2L-CNN; (b) 2Ls-CNN architectures

4 stories. Thus, the MPR variation, which was utilized as input data for CNN, was a 12 × 12 square; this enabled the same architecture to be used for the CNN as described in the Section 2.2. As discussed in the Section 3, each node of the output layer included the stiffness reduction data of each floor (DOF) and thus the number of nodes was the same as that of the considered DOF. On the other hand, in the output layer of the CNN architecture for the ASCE model, the number of nodes was set to be the same as that of the brace groups where stiffness could be reduced, i.e., a damage was expected to occur, such that each node in the output layer contained the damage information of each brace group.

Table 2 Details of the additional CNN architectures

Case	CNN label	Layer No.	Depth	Kernel size	Subsampling size
1	CNN-2L	1	12	5	2
		2	24	3	2
2	CNN-2Ls	1	12	5	2
		2	24	3	1
3	CNN-2Lk	1	12	3	2
		2	24	2	2
4	CNN-2Lc	1	12	3	2
		2	24	2	1
5	CNN-3Ls	1	12	5	2
		2	24	3	1
		3	36	1	1
6	CNN-3Lk	1	12	3	2
		2	24	2	2
		3	36	1	2
7	CNN-3Lc	1	12	3	2
		2	24	2	1
		3	36	1	1

4.2 Results and discussion

The presented CNN architecture and 3000 training datasets from the total of 3100 datasets, which were created from the abovementioned damage scenarios, were used to train the CNN for damage detection in the ASCE benchmark model. The remaining 100 datasets, which were not used for CNN training, were used to verify the damage detection performance of the trained CNN. For the 100 verification datasets, the RMSE was 1.1885 and average absolute error was 0.5259.

Fig. 9(a) shows the results of the five most unfavorable cases with highest prediction errors in terms of absolute error among the 100 verification datasets. For the 100 verification datasets, the overall performance for detecting damage location and damage severity was observed to be good. However, for the five most unfavorable cases, faulty detection was observed in terms of both damage location and damage severity. In particular, the Cases 1–3 in Fig. 9(a) showed absolute errors ranging from 10.64 to 16.14, which indicates underestimation (red circle in Fig. 9(a)). In addition, the Cases 4 and 5 in Fig. 9(a) showed faulty detection, failing to identify even the damage locations.

To avoid those faulty detections and find the architecture with better performance in damage detection, the influences of variations in the parameters in the CNN layers, which were discussed in Section 2, as well as the number of layers on the performance of the CNN were examined. Six additional CNN architectures were evaluated, details for which are listed in Table 2.

Case 1 in Table 2 is the basic architecture used for damage detection, which is designated as 2L-CNN, where 2L indicates two layers. Then, Cases 2–4 have two layers, while Cases 5–7 have three layers. The CNN architectures with three layers involve connecting the third convolutional layer to the last pooling layer of the two-layer architectures, which is shown in Fig. 3, followed by the third pooling layer that was connected to FC layer, which is eventually connected to the output layer. Fig. 10 shows the basic form

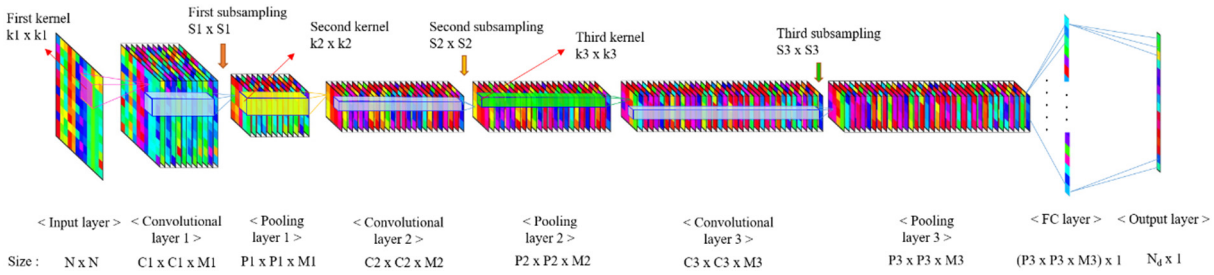

Fig. 10 CNN architecture with three layers (CNN-3Lc)

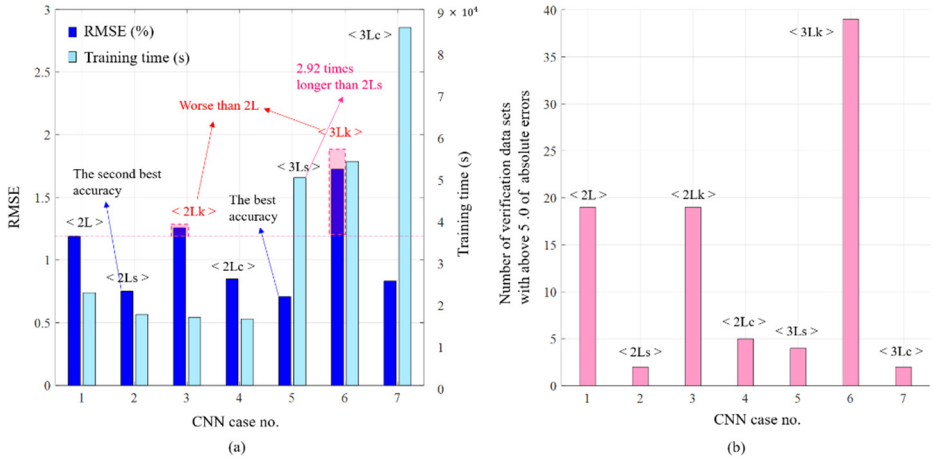

Fig. 11 Comparisons of the different CNN architectures in terms of (a) RMSE and training time; (b) number of verification cases exceeding a 5.0 of absolute error

of the three-layer CNN architecture.

Considering the labels of each architecture in Table 2, 's' indicates that the subsampling size was reduced below 2L-CNN, which represents the basic architecture. During subsampling, the value of the stride size is identical to that of subsampling size. Furthermore, 'k' indicates that the kernel size was decreased below 2L-CNN, while 'c' indicates that both subsampling size and kernel size were reduced.

The seven CNN architectures listed in Table 2, which includes the basic CNN architecture (2L-CNN (Case 1)), were used for damage detection in the ASCE benchmark model; the obtained results were compared in terms of damage detection performance. Under the same conditions as the damage scenario discussed in the previous section, 3000 datasets from among the 3100 generated datasets were used to train the CNNs, while the remaining 100 datasets were used for verification. Fig. 11(a) shows the RMSE errors of the seven CNN architectures for the 100 verification datasets; the training time is also presented in Fig. 11(a). Aside from 2Lk-CNN and 3Lk-CNN architectures, which had reduced kernel sizes, the remaining CNN architectures showed better accuracy than the 2L-CNN architecture for damage detection in the ASCE benchmark model.

Furthermore, the comparison between 2L-CNN and 2Lk-CNN revealed that the reduction of kernel size, which was used to construct convolutional layers, degraded the performance of CNN at least considering the scenario explored in our study.

In addition, on comparing the 2L-CNN architecture with the 2Ls-CNN architecture, it is clear that the decrease in the subsampling size of the pooling layer improved the performance of the CNN. In addition, both 2Lc-CNN and 3Lc-CNN architectures, which included both reduced kernel and subsampling sizes, showed better performance compared with the basic architecture (2L-CNN). Nevertheless, their damage detection performance was worse than that of the 2Ls-CNN and 3Ls-CNN architectures; this can be attributed to the reduction of subsampling size serving as an offset to the reduction of the kernel size.

In terms of RMSE, the 3Ls-CNN architecture showed the best performance for damage detection. The 3Ls-CNN architecture achieved a 5.69% reduction in RMSE compared with that of the 2Ls-CNN. The training time of 3Ls-CNN was 2.92 times that of the 2Ls-CNN architecture. The overall accuracy of damage detection for the 100 verification sets was evaluated in terms of the RMSE, while the prediction performance of each verification set was assessed by checking whether each verification set exceeded the absolute error of 5%. Fig. 11(b) graphically shows the number of verification sets that exceeded the 5.0 of absolute error for the seven CNN architectures, among the 100 verification sets. The overall trend in Fig. 11(b) was similar to that of the RMSE in Fig. 11(a). However, for the 3Ls-CNN architecture, which showed the highest accuracy in terms of RMSE, four verification sets exceeding the 5.0 of absolute error were observed, while for the 2Ls-CNN architecture just had two verification sets exceeding the 5%

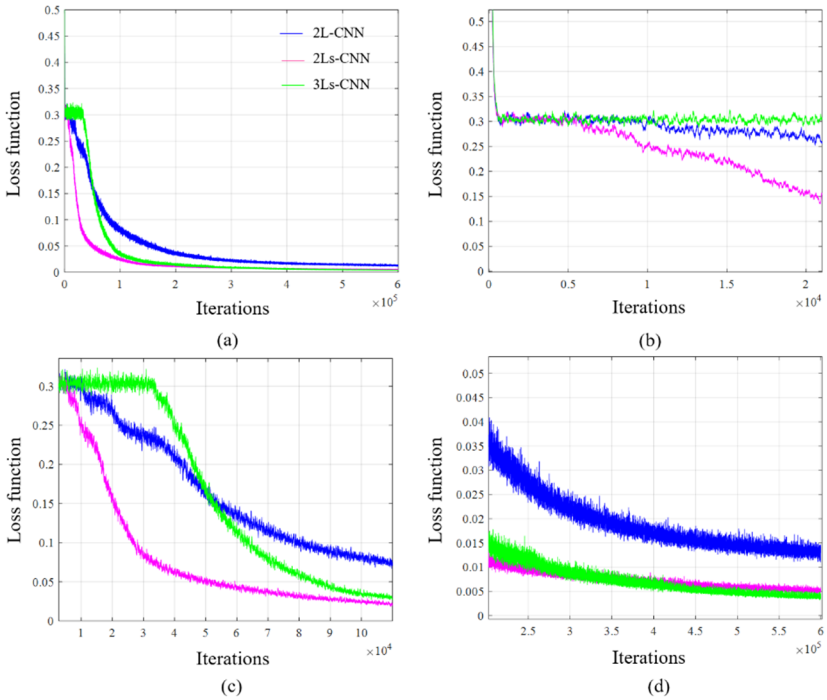

Fig. 12 Convergence curves for 2L-CNN, 2Ls-CNN, and 3Ls-CNN architectures. (a) iterations from 0 to 600000; (b) iterations from 0 to 20000; (c) iterations from 10000 to 100000; (d) iterations from 200000 to 600000

absolute error were observed. In the case of the 3Ls-CNN architecture, one case among the four cases exceeding the 5% absolute error was found to be a faulty detection.

Based on the above comparisons, when the prediction performance for all verification sets, computational cost, as well as prediction performance for each verification set are comprehensively considered, one of the most efficient CNN architectures can be regarded as the 2Ls-CNN architecture. Fig. 9(b) shows the damage detection result of the 2Ls-CNN architecture for the five most unfavorable verification sets, which were presented to verify the performance of the basic CNN architecture. The faulty detection and underestimation of damage severity in the case of the 2L-CNN architecture, which was shown in Fig. 9(a), significantly improved in the prediction result of the 2Ls-CNN architecture. In addition, the average absolute difference of damage cases below 10% of stiffness reduction ratio was about 1.7 times higher than that of damage cases above 20% of stiffness reduction ratio in the 2Ls-CNN results. It indicates that the 2Ls-CNN predicts more precisely moderate damage case which is more important in assessment of structural health; thus, the presented model can be evaluated to be effective in terms of practical implementation for damage detection.

The convergence characteristics of the presented CNN architecture were examined during training. Fig. 12(a) shows the convergence curves of the 2L-CNN, 2Ls-CNN, and 3Ls-CNN architectures; these CNN architectures had convergences with remarkably different features. As shown in Fig. 12(b), all the three architectures converged in a steep slope around 700 of iterations. Until about 5000 of iterations, the three architectures were trained showing similar values for the loss function. After that, the 2Ls-CNN architecture converged by reducing the value of the loss function with a steeper slope compared with 2L-CNN and 3Ls-CNN. As Fig. 12(c) shows, the 2Ls-CNN architecture featured an earlier and faster convergence, while the 3Ls-CNN architecture had a slower convergence by showing only few improvements in the value of loss function until 40000 of iterations. This figure also shows that 3Ls-CNN, which is the best architecture in terms of RMSE, has worse performance compared with 2L-CNN if the number of iterations does not exceed 50000. As shown in Fig. 12(d), the loss function value of the 3Ls-CNN architecture did not become lower than that of the 2Ls-CNN architecture until about 350000 of iterations. Although the CNN with three layers required a much longer time for one training than the CNN with two layers, the analysis of the convergence curves indicates that, unless the CNN with three layers is sufficiently trained, it would have a worse performance than the CNN with two layers, which has similar training operator characteristics.

5. Conclusions

This study presents a CNN-based damage detection method for building structures, which uses MPRs extracted from modal responses of the structures. In particular, time history structural responses measured for a sufficient time in a building structure under ambient excitation conditions are transformed to MPRs indicating the measuring points and considered modes. In the transformation process, a robust and fast filtering of measured responses considering modes to be interest is employed to extract modal responses by removing noise effects from field tests resulting better reflection of modal behaviors to modal responses and MPR. In addition, as the responses used in the method are

measured under ambient excitation, no loading acting on the target building is required. Furthermore, as MPRs are directly extracted from measured responses in a relatively simple way, the conventional identification process of modal parameters which can be considerably influenced by various uncertain factors around the building is not required. By establishing the MPR variations obtained from comparisons of MPRs between healthy and damaged structures in the input map of the CNN considering the number of measuring points and modes, the presented CNN model produces the damage locations and damage severities as output data, which are expressed by stiffness reduction in this method. Based on the Big Data concept, numerous datasets with such input-output relationships are created based on predefined damage scenarios, which are used for CNN training. A CNN architecture, which consists of two convolutional and two pooling layers as well as a FC and output layer, was presented and applied to detect damages in the case of two MDOFs. The presented method showed good performance in the case of both single and multiple damage detections. The increase in the number of training datasets used for CNN training improved the performance of damage detection. However, the computational cost for training also increased. The presented method was applied to multiple damage detection for a 3-D ASCE benchmark model. Using the CNN trained with multiple training datasets, damage locations and severities could be detected. In the results, faulty detections were observed in some verification datasets. A comparative study was conducted for damage detection in the ASCE benchmark model for architectures with different operator sizes and number of layers in the CNN. It was observed that a decreased kernel size for building convolutional layers degraded the damage detection performance of the CNN. In contrast, a decreased subsampling size of the pooling layer improved the damage detection performance. Furthermore, an increase in the number of layer improved the performance of the CNN with a reduction of 5.69% in RMSE, but increased the computational cost by 2.92 times from the comparison of results between 2Ls-CNN and 3Ls-CNN. A 2Ls-CNN which is one of the most efficient architectures derived from the comparative study showed better results with RMSE of 0.7513 and 2% of faulty detection than other and has one life cycle, there is a limitation in the implementation of the presented method based on the supervised learning, which requires damage simulations for the structures to obtain data. To overcome the limitation, the precise model for the healthy state of the structure can be derived by minimizing the discrepancy between the model and measurement, and then utilized to create data of damaged states of the structure by varying the stiffness of the elements of the model. The created data, in turn, can be utilized in the training of the presented CNN.

Acknowledgments

This work was supported by a National Research Foundation of Korea (NRF) grant funded by the Korea government (Ministry of Science, ICT & Future Planning, MSIP) (NRF-2021R1A2C33008989 and No. 2018R1A5A1025137).

References

Abdeljaber, O., Avci, O., Kiranyaz, S., Gabbouj, M. and Inman, D.J. (2017), "Real-time vibration-based structural damage detection using one-dimensional convolutional neural networks", *J. Sound Vib.*, **388**, 154-170. https://doi.org/10.1016/j.jsv.2016.10.043

Abdeljaber, O., Avci, O., Kiranyaz, M.S., Boashash, B., Sodano, H. and Inman, D.J. (2018), "1-D CNNS for structural damage detection: Verification on a structural health monitoring benchmark data", *Neurocomputing*, **275**, 1308-1317. https://doi.org/10.1016/j.neucom.2017.09.069

Chen, F. and Jahanshahi, M.R. (2018), "NB-CNN: Deep learning-based crack detection using convolutional neural network and Naive Bayes data fusion", *IEEE Trans Ind. Electron.*, **65**(5), 4392-4400. https://doi.org/10.1109/TIE.2017.2764844

Chen, J. and Loh, C. (2018), "Two-stage damage detection algorithms of structure using modal parameters identified from recursive subspace identification", *Earthq. Eng. Struct. D.*, **47**(3), 573-593. https://doi.org/10.1002/eqe.2980

Chen, C., Jiang, F., Yang, C., Rho, S., Shen, W., Liu, S. and Liu, Z. (2018), "Hyperspectral classification based on spectral-spatial convolutional neural networks", *Eng. Appl. Artif. Intell.*, **68**, 165-171. https://doi.org/10.1016/j.engappai.2017.10.015

Chopra, A.K. (2001), *Dynamics of Structures - Theory and Applications to Earthquake Engineering*, Pearson, Englewood Cliffs, NJ, USA.

Esfandiari, A. (2017), "An innovative sensitivity-based method for structural model updating using incomplete modal data", *Struct. Control Hlth.*, **24**(4), e1905. https://doi.org/10.1002/stc.1905

Glisic, B. and Inaudi, D. (2012), "Development of method for in-service crack detection based on distributed fiber optic sensors", *Struct. Health Monit.*, **11**(2), 161-171. https://doi.org/10.1177/1475921711414233

Glisic, B., Inaudi, D., Lau, J.M. and Fong, C.C. (2013), "Ten-year monitoring of high-rise building columns using long-gauge fiber optic sensors", *Smart Mater. Struct.*, **22**(5), 055030. https://doi.org/10.1088/0964-1726/22/5/055030

Guo, Y.L., Kwon, D.K. and Kareem, A. (2016), "Near-real-time hybrid system identification framework for civil structures with application to Burj Khalifa", *J. Struct. Eng.*, **142**(2), 04015132. https://doi.org/10.1061/(ASCE)ST.1943-541X.0001402

Hsu, T.Y., Liao, W.I. and Hsiao, S.Y. (2017), "Damage detection for beam structures based on local flexibility method and macro-strain measurement", *Smart Struct. Syst.*, *Int. J.*, **19**(4), 393-402. https://doi.org/10.12989/sss.2017.19.4.393

Johnson, E.A., Lam, H.F., Katafygiotis, L.S. and Beck, J.L. (2004), "Phase I IASC-ASCE structural health monitoring benchmark problem using simulated data", *J. Eng. Mech.*, **130**(1), 3-15. https://doi.org/10.1061/(ASCE)0733-9399(2004)130:1(3)

Kaveh, A. and Maniat, M. (2015), "Damage detection based on MCSS and PSO using modal data", *Smart Struct. Syst.*, *Int. J.*, **15**(5), 1253-1270. https://doi.org/10.12989/sss.2015.15.5.1253

Lecun, Y., Bengio, Y. and Hinton, G. (2015), "Deep learning", *Nature*, **521**(7553), 436-444. https://doi.org/10.1038/nature14539

Li, J. and Hao, H. (2014), "Substructure damage identification based on wavelet-domain response reconstruction", *Struct. Health Monitor.*, **13**(4), 389-405. https://doi.org/10.1177/1475921714532991

Li, P., Zhu, H., Luo, H. and Weng, S. (2015), "Structural damage identification based on genetically trained ANNs in beams",

Smart Struct. Syst., Int. J., **15**(1), 227-244. http://dx.doi.org/10.12989/sss.2015.15.1.227

Li, Z., Park, H.S. and Adeli, H. (2017), "New method for modal identification of super high-rise building structures using discretized synchrosqueezed wavelet and Hilbert transforms", *Des. Tall Spec.*, **26**(3), 273-289. https://doi.org/10.1002/tal.1312

Liang, Y., Li, D., Song, G. and Zhan, C. (2017), "Damage detection of shear buildings through structural mass-stiffness distribution", *Smart Struct. Syst.*, *Int. J.*, **19**(1), 11-20. http://dx.doi.org/10.12989/sss.2017.19.1.011

Liang, Y., Feng, Q., Li, H. and Jiang, J. (2019), "Damage detection of shear buildings frequency-change-ratio and model updating algorithm", *Smart Struct. Syst.*, *Int. J.*, **23**(2), 107-122. http://dx.doi.org/10.12989/sss.2019.23.2.107

Lin, Y.Z., Nie, Z.H. and Ma, H.W. (2017), "Structural damage detection with automatic feature-extraction through deep learning", *Comput.-Aided Civil Inf.*, **32**(12), 1025-1046. https://doi.org/10.1111/mice.12313

Machavaram, R. and Shankar, K. (2013), "Joint damage identification using improved radial basis function networks in frequency and time domain", *Appl. Soft Comput.*, **13**(7), 3366-3379. https://doi.org/10.1016/j.asoc.2013.02.004.

Oh, B.K., Hwang, J.W., Kim, Y., Cho, T. and Park, H.S. (2015), "Vision-based system identification method for building structures using a motion capture system", *J. Sound Vib.*, **356**, 72-85. https://doi.org/10.1016/j.jsv.2015.07.011

Oh, B.K., Kim, D. and Park, H.S. (2017), "Modal response-based visual system identification and model updating methods for building structures", *Comput.-Aided Civil Inf.*, **32**(1), 34-56. https://doi.org/10.1111/mice.12229

Oppenheim, A.V. and Schafer, R.W. (2011), *Discrete-Time Signal Processing*, Pearson, Upper Saddle River, NJ, US.

Pacific Earthquake Engineering Research Center (PEER) (2006), OpenSees: Open System for Earthquake Engineering Simulation, University of California, CA, USA.

Padil, K.H., Bakhary, N. and Hao, H. (2017), "The use of a non-probabilistic artificial neural network to consider uncertainties in vibration-based-damage detection", *Mech. Syst. Signal Pr.*, **83**, 194-209. https://doi.org/10.1016/j.ymssp.2016.06.007

Park, H.S. and Oh, B.K. (2018a), "Real-time structural health monitoring of a supertall building under construction based on visual modal identification strategy", *Automat. Constr.*, **85**, 273-289. https://doi.org/10.1016/j.autcon.2017.10.025

Park, H.S. and Oh, B.K. (2018b), "Damage detection of building structures under ambient excitation through the analysis of the relationship between the modal participation ratio and story stiffness", *J. Sound Vib.*, **418**, 122-143. https://doi.org/10.1016/j.jsv.2017.12.036

Park, S.W., Park, H.S., Kim, J.H. and Adeli, H. (2015), "3d displacement measurement model for health monitoring of structures using a motion capture system", *Measurement*, **59**, 352-362. https://doi.org/10.1016/j.measurement.2014.09.063

Park, H.S., Kim, D., Lim, S.A. and Oh, B.K. (2017), "Dynamic torsional response measurement model using motion capture system", *Smart Struct. Syst., Int. J.*, **19**(6), 679-694. http://dx.doi.org/10.12989/sss.2017.19.6.679

Park, S., Jeong, H., Min, H., Lee, H. and Lee, S. (2018), "Wavelet-like convolutional neural network structure for time-series data classification", *Smart Struct. Syst., Int. J.*, **22**(2), 175-183. http://dx.doi.org/10.12989/sss.2018.22.2.175

Sarlo, R., Tarazaga, P.A. and Kasarda, M.E. (2018), "High resolution operational modal analysis on a five-story smart building under wind and human induced excitation", *Eng. Struct.*, **176**, 279-292. https://doi.org/10.1016/j.engstruct.2018.08.060

Sigurdardottir, D.H. and Glisic, B. (2015), "On-Site Validation of Fiber-Optic Methods for Structural Health Monitoring: Streicker Bridge", *J. Civil Struct. Health Monitor.*, **5**(4), 529-549. https://doi.org/10.1007/s13349-015-0123-x

Sigurdardottir, D.H. and Glisic, B. (2014), "Detecting minute damage in beam-like structures using the neutral axis location", *Smart Mater. Struct.*, **23**(12), 125042. https://doi:10.1088/0964-1726/23/12/125042

Sotoudehnia, E., Shahabian, F. and Sani, A.A. (2019), "An iterative method for damage identification of skeletal structures utilizing biconjugate gradient method and reduction of search space", *Smart Struct. Syst., Int. J.*, **23**(1), 45-60. http://dx.doi.org/10.12989/sss.2019.23.1.045

Sun, S.B., He, Y.Y., Zhou, S.D. and Yue, Z.J. (2017), "A data-driven response virtual sensor technique with partial vibration measurements using convolutional neural network", *Sensors*, **17**(12), 2888. https://doi.org/10.3390/s17122888

Wu, W.H., Chen, C.C., Jhou, J.W. and Lai, G. (2018), "A rapidly convergent empirical mode decomposition method for analyzing the environmental temperature effects on stay cable force", *Comput.-Aided Civil Inf.*, **33**(8), 672-690. https://doi.org/10.1111/mice.12355

Xiong, H., Cao, J., Zhang, F., Ou, X. and Chen, C. (2019), "Investigation of the SHM-oriented model and dynamic characteristics of a super-tall building", *Smart Struct. Syst., Int. J.*, **23**(3), 295-306. http://dx.doi.org/10.12989/sss.2019.23.3.295

Xu, B., Song, G. and Masri, S.F. (2011), "Damage detection for a frame structure model using vibration displacement measurement", *Struct. Health Monitor.*, **11**(3), 281-292. http://doi.org/10.1177/1475921711430437

Xu, Y., Bao, Y., Chen, J., Zuo, W. and Li, H. (2018), "Surface fatigue crack identification in steel box girder of bridges by a deep fusion convolutional neural network based on consumer-grade camera images", *Struct. Health Monitor.*, **18**(3), 653-674. https://doi.org/10.1177/1475921718764873

Yin, T., Jiang, Q. and Yuen, K. (2017), "Vibration-based damage detection for structural connections using incomplete modal data by Bayesian approach and model reduction technique", *Eng. Struct.*, **132**, 260-277. https://doi.org/10.1016/j.engstruct.2016.11.035

Zhang, C.D. and Xu, Y.L. (2016), "Structural damage identification via multi-type sensors and response reconstruction", *Struct. Health Monitir.*, **15**(6), 715-729. https://doi.org/10.1177/1475921716659787

Zhang, F.L., Xiong, H.B., Shi, W.X. and Ou, X. (2016), "Structural health monitoring of Shanghai Tower during different stages using a Bayesian approach", *Struct. Control Hlth.*, **23**(11), 1366-1384. https://doi.org/10.1002/stc.1840

Zhu, Y.C., Xie, Y.L. and Au, S.K. (2018), "Operational modal analysis of an eight-storey building with asynchronous data incorporating multiple setups", *Eng. Struct.*, **165**, 50-62. https://doi.org/10.1016/j.engstruct.2018.03.011

HJ